Available online at www.sciencedirect.com
ScienceDirect
Journal of Molecular Catalysis A: Chemical 272 (2007) 96–107
JOURNAL OF MOLECULAR CATALYSIS A: CHEMICAL
www.elsevier.com/locate/molcata

A characterization of Ln-Pd/SiO_2 (Ln=La, Ce, Sm, Eu, Gd and Yb): Correlation of surface chemistry with hydrogenolysis activity

Satyakrishna Jujjuri [a], Errun Ding [b], Sheldon G. Shore [b], Mark A. Keane [c,*]

[a] *Department of Chemical and Materials Engineering, University of Kentucky, Lexington, USA*
[b] *Department of Chemistry, The Ohio State University, Columbus, USA*
[c] *Chemical Engineering, School of Engineering and Physical Sciences, Heriot-Watt University, Edinburgh EH14 4AS, Scotland*

Received 2 February 2007; accepted 3 March 2007
Available online 12 March 2007

Abstract

The gas phase hydrodechlorination (HDC) of chlorobenzene (CB), 1,2-dichlorobenzene (1,2-DCB) and 1,3-dichlorobenzene (1,3-DCB) has been investigated over Pd/SiO_2 and a series of Ln-Pd/SiO_2 prepared from the organometallic precursor $\{(DMF)_{10}Ln_2[Pd(CN)_4]_3\}_\infty$ where Ln = La, Ce, Sm, Eu, Gd and Yb; Pd loading = 5%, w/w. Under identical reaction conditions, the following overall sequence of increasing initial fractional dechlorination has been established: Pd/SiO_2 < Yb-Pd/SiO_2 ≈ Sm-Pd/SiO_2 < Gd-Pd/SiO_2 < La-Pd/SiO_2 ≈ Ce-Pd/SiO_2 < Eu-Pd/SiO_2; reaction over Ln/SiO_2 resulted in a negligible conversion. HDC activity declined with time-on-stream but the Ln-Pd/SiO_2 catalysts maintained a significantly higher fractional HDC than Pd/SiO_2; loss of activity is attributed to deleterious HCl/surface interactions. The pre- and post- reaction catalyst samples have been characterized in terms of BET area, TPR, TEM, H_2 chemisorption/TPD, XRD and XPS analyses. When compared with Pd/SiO_2, Pd is present in the Ln-Pd/SiO_2 samples as much smaller particles, while the lanthanide component is finely dispersed over the surface, i.e. Ln is in intimate contact with Pd. The promotional effect of Ln in Ln-Pd/SiO_2 is attributed to a surface Pd/Ln synergism resulting in an enhancement of surface reactive hydrogen and a more effective C–Cl bond activation for hydrogenolytic attack. HDC performance is discussed in terms of surface composition, Pd particle size, Ln electronic structure and H_2 uptake/release dynamics.

Keywords: Hydrodechlorination; Pd/SiO_2; Ln-Pd/SiO_2; Lanthanide hydrides; Chlorobenzene(s); Catalyst deactivation

1. Introduction

Chlorinated effluents are a major threat to our environment due to their toxic/carcinogenic nature, negative impact on the biosphere and participation in stratospheric reactions that deplete the ozone layer [1–3]. While a concerted effort is now in place to minimize chloroarene use (as solvents and in the synthesis of pesticides, lubricants, pharmaceuticals, glues and paints), in many instances they are irreplaceable and new efficient approaches are called for that will serve to detoxify chloroarene waste streams [4]. A detoxification process that can facilitate the recycle of the parent aromatic and/or a target partially chlorinated aromatic represents a progressive green processing approach. Catalytic hydrodechlorination (HDC) is now viewed as a viable means of achieving this goal [5]. Catalysts employed in gas phase HDC applications typically suffer a serious decline in activity with time-on-stream [6–12], which has been attributed to surface Cl interaction(s) that serve(s) to poison the active metal [7,8,10]. The development of solid HDC catalysts that exhibit high and stable activities and a tuneable selectivity represents a challenging problem in heterogeneous catalysis. Group VIII noble metals are known to be effective in hydrogenolysis and Pd has been demonstrated to deliver the highest specific HDC rates [6,13]. Moreover, HDC performance has been shown to be sensitive to Pd dispersion and the nature of the support [14–16]. In two previous publications [17,18], we established that HDC over Yb-Pd/SiO_2 (prepared from a $\{(DMF)_{10}Yb_2[Pd(CN)_4]_3\}_\infty$ precursor) proceeded at an appreciably higher rate than that delivered by a conventional Pd/SiO_2. The source of the Yb promotional effect was ascribed to a greater quantity of surface hydrogen associated with the bimetallic samples that is the result of a Yb/Pd synergism involving hydride

* Corresponding author. Tel.: +44 131 4514719.
E-mail address: M.A.Keane@hw.ac.uk (M.A. Keane).

1381-1169/$ – see front matter © 2007 Elsevier B.V. All rights reserved.
doi:10.1016/j.molcata.2007.03.008

formation/H_2 transfer. It must be stressed that the positive influence of Yb is not limited to hydrogenolysis in that we have established enhanced aromatic hydrogenation activity for Yb-Pd/SiO_2 when compared with Pd/SiO_2 [19,20]. In this study, we extend the work further by considering the action of a series of silica supported Ln-Pd (Ln = La, Ce, Sm, Eu, Gd and Yb) catalysts prepared from analogous Pd-Ln organometallic complex precursors. This series of lanthanide metals has been chosen to facilitate an assessment of electronic effects (variation in valence shell electrons) and possible differences in hydride response in determining HDC performance for the conversion of chlorobenzene (CB), 1,2- and 1,3- dichlorobenzene (DCB). A lanthanide promotion of transition metal catalysts has been established elsewhere in a number of applications [21–26] and attributed to electron-transfer [21,22,26], metal particle size effects [22], hydrogen transfer [23] and intermetallide formation [25]. The lanthanide component has been reported to exist as discrete particles/ensembles [25], to encapsulate the Pd particles [22] or to form a continuous film in the case of our preparation with the $\{(DMF)_{10}Yb_2[Pd(CN)_4]_3\}_\infty$ precursor [18–20]. While homogeneous lanthanide catalysts have been used in liquid phase haloarene dehalogenation [27,28], a systematic search failed to unearth any comprehensive study of gas phase HDC promoted by Ln-Pd systems. This paper represents the first recorded use of a range of Ln-Pd/SiO_2 that will supplement the burgeoning literature on catalytic HDC. The catalysts, pre- and post-reaction, have been characterized by a range of complementary techniques (BET/TPR, H_2 chemisorption/TPD, XRD, TEM and XPS) in order to gain some insight into the relationship between catalyst structure and catalytic activity.

2. Experimental

2.1. Catalyst preparation and activation

The Pd/Ln complexes $\{(DMF)_{10}Ln_2[Pd(CN)_4]_3\}_\infty$, (Ln = La, Ce, Sm, Eu, Gd and Yb) which served as the bimetallic catalyst precursors were prepared using a procedure previously described by Shore and co-workers [29]. A solution of the bimetallic complex in DMF (dimethyl formamide) was contacted with a sample of fumed SiO_2 to deliver a 5%, w/w, Pd loading. The DMF was removed from the metal impregnated SiO_2 under vacuum over a period of 12 h at room temperature. The resulting solid was removed in air and placed (in a quartz boat) in a furnace, contacted with H_2 for ca. 10 min and reduced under a steady H_2 flow at 10 K min^{-1}, to a final temperature of 523 K which was maintained for 30 min. The sample was then flushed in He and passivated in a 1%, v/v, O_2 in He flow at room temperature. A monometallic 5%, w/w, Pd/SiO_2 was prepared by contacting the same SiO_2 substrate with the acetate precursor (in DMF) with subsequent activation/passivation as above; details are provided elsewhere [19]. Monometallic 5%, w/w, Ce, Eu and Yb on SiO_2 were prepared by charging known amounts of SiO_2 and the metal powder into a reaction flask (located in a dry box) with vacuum transfer of liquid ammonia into the flask at 195 K. The mixture was kept under constant agitation for ca. 3 h at which point the liquid ammonia was pumped away: the catalyst precursors were reduced and passivated as above. Each sample was sieved (ATM fine test sieves) into a batch of 75 μm average particle diameter and subjected to a second reduction step (prior to catalysis) in a fixed bed tubular glass reactor (i.d. = 1.25 cm) by heating (10 K min^{-1}) in a 60 cm^3 min^{-1} stream of dry H_2 (99.999%), monitored using a Humonics (Model 520) flow meter to a final temperature of 573 K that was maintained for 12 h.

The BET surface area, temperature programmed reduction (TPR), H_2 chemisorption and temperature programmed desorption (TPD) associated with the freshly activated and spent samples were determined using the commercial CHEM-BET 3000 (Quantachrome) unit. The samples (ca. 0.1 g) were loaded in a U-shaped Pyrex/Quartz glass cell (21 cm × 3.76 mm i.d.). The total surface area was recorded in a 30%, v/v, N_2/He flow; pure N_2 (99.9%) served as the internal standard. After outgas for 30 min, at least two cycles of N_2 adsorption–desorption in the flow mode were employed using the standard single point BET method. TPR was performed in 20 cm^3 min^{-1} (Brooks mass flow controller) 5%, v/v, H_2/N_2 to 573 K at 10 K min^{-1} and the effluent gas passed through a liquid N_2 trap; H_2 consumption was monitored by a thermal conductivity detector (TCD) with data acquisition/manipulation using the TPR Win™ software. The samples were swept with 20 cm^3 min^{-1} dry N_2 for 1 h at 573 K, cooled to room temperature and subjected to H_2 chemisorption using a pulse (50 μl) titration procedure. Any possible contribution due to β-palladium hydride formation was avoided as the H_2 partial pressure <2 Torr, i.e. well below the pressure (>11 Torr) required to generate the hydride [8]. The sample was thoroughly flushed with pure N_2 (20 cm^3 min^{-1}) for 30 min to remove any weakly bound hydrogen. Temperature programmed desorption (TPD) was conducted in the N_2 flow at 50 K min^{-1} to 1273 K with an isothermal hold of 15 min. Based on TCD calibrations and analysis of the effluent gas using a MICROMASS PC Residual Gas Analyser, the TPD profiles recorded in this paper can be positively attributed solely to H_2 release. BET surface area and H_2 uptake values were reproducible to within ±5% and the values quoted in this paper are the mean. The nature of the surface Pd/Ln phase was probed by transmission electron microscopy (TEM) analysis which was carried out using a JEOL-2000 TEM/STEM microscope equipped with a UTW energy dispersive X-ray (EDX) detector (Oxford Instruments) and operated at an accelerating voltage of 200 kV. The specimens were prepared by ultrasonic dispersion in 2-butanol, evaporating a drop of the resultant suspension onto a holey carbon support grid. The surface weighted Pd particle sizes (d_s) quoted in this study are based on a measurement of up to 750 individual particles, where

$$\bar{d}_s = \frac{\sum n_i d_i^3}{\sum n_i d_i^2} \quad (1)$$

X-ray powder data were collected on a Bruker D8 Advance X-ray powder diffractometer (Cu Kα radiation) from samples (subjected to a reductive atmosphere at 523 K) loaded in 0.5 mm Lindeman glass capillaries in a glove box and sealed. X-ray

photoelectron spectroscopic (XPS) analyses were conducted using a Kratos Axis Ultra spectrometer with monochromatized Mg Kα radiation (1253.6 eV). A sample of activated/passivated catalyst was adhered to a conducting carbon tape, mounted in the sample holder and subjected to UHV conditions (~10^{-9} Torr) overnight prior to analysis. Full range surveys (0–1000 eV) and high resolution spectra (range of ~30 eV) of Pd $3d_{5/2}$, Ce $3d_{5/2}$, Eu $3d_{5/2}$, Yb $4d_{5/2}$, Si 2p, O 1s, Cl $2p_{3/2}$ and C 1s were collected. The C 1s peak, centered at 284.5 eV served as reference to calibrate the binding energy values. The signals for Pd, Ce, Eu, Yb and Cl were much weaker than Si and O, due to the low concentrations in the SiO_2 matrix with the result that extended scans were employed to improve the signal/noise ratio.

2.2. Catalytic system

The reactions were conducted *in situ* (after catalyst activation) with a co-current flow of the chloroarene feed in H_2. A layer of glass beads above the catalyst bed ensured that the reactants were vaporized and reached reaction temperature before contacting the catalyst [30]. A Model 100 (kd Scientific) microprocessor controlled infusion pump was used to deliver the aromatic feed, *via* a glass/teflon air-tight syringe and teflon line at a fixed calibrated flow rate, which was carried through the catalyst bed in a stream of dry H_2. All the HDC reactions were carried out at an inlet hourly Cl/Pd mole ratio = 5×10^3, contact time = 0.02 min and 423 K where isothermal (423 K) operation was ensured by diluting the catalyst bed with ground glass (75 μm). The ground glass was mixed thoroughly with catalyst before insertion into the reactor. In a series of blank tests, passage of each reactant in a stream of H_2 through the empty reactor, i.e. in the absence of catalyst, did not result in any detectable conversion. The reactor effluent was frozen in a liquid nitrogen trap for subsequent analysis which was made using a Perkin-Elmer Auto System XL chromatograph equipped with a split/splitless injector and a flame ionization detector, employing a DB-1 50 m × 0.20 mm i.d., 0.33 μm capillary column (J&W Scientific). The overall level of HDC was converted to mol% conversion using detailed calibration plots for each feedstock. Quantitative analysis was based on relative peak area with acetone as solvent where analytical repeatability was better than ±0.4% and the detection limit typically corresponded to a feedstock conversion less than 0.1 mol%. HDC performance is quantified in terms of fractional dechlorination (x_{Cl})

$$x_{Cl} = \frac{[Cl]_{in} - [Cl]_{out}}{[Cl]_{in}} \quad (2)$$

where it has been demonstrated previously [30–32] that HCl is the only inorganic product with no detectable Cl_2 production. The percentage selectivity of benzene ($S_{benzene}$%) from either DCB feed is given by

$$S_{benzene}\% = \frac{[benzene]_{out}}{[DCB]_{in} - [DCB]_{out}} \times 100 \quad (3)$$

Temporal changes in x_{Cl} are expressed in this paper in terms of the empirical first order exponential decay equation

$$x_{Cl} = x_0 - \alpha(1 - e^{-\beta \Delta t}) \quad (4)$$

where x_0 represents the initial fractional HDC, α and β are pre-exponential and inverse time fitting parameters, respectively. All the chemicals in this study were supplied by Sigma–Aldrich (≥99.8%, v/v) and were used without further purification. Repeated reactions with different samples from the same batch of catalysts delivered product compositions that were reproducible to better than ±5 %.

3. Results and Discussion

3.1. Catalyst characterization: pre-HDC

3.1.1. BET/TPR/XRD

The BET surface areas of the unused (pre-HDC) catalysts are recorded in Table 1. While Pd/SiO_2 exhibited a BET area similar to that of the support (200 $m^2\ g^{-1}$), each of the Ln/SiO_2 samples possessed significantly lower (160–183 $m^2\ g^{-1}$) areas, which can be attributed to a partial pore filling during sample preparation. This effect extends to the Ln-Pd/SiO_2 samples as is evident from the entries in Table 1. The TPR profiles associated with each of the passivated samples are shown in Fig. 1. The profiles are dominated, in every case, by a negative peak at 366 ± 6 K representing H_2 release which can be attributed to the decomposition of β-Pd hydride that is known to occur over the temperature range of 323–373 K [22,33–37]. The absence of any obvious H_2 consumption in advance of H_2 release presupposes the existence of the metallic phase prior to the commencement

Table 1
BET surface areas, temperature related peak maxima (T_{max}) associated with the TPR profiles, H/Pd mol ratios corresponding to β-hydride decomposition (T_{max} given in bold), H_2 uptake and corresponding H_2 release (over *T* range I identified in Fig. 4) for the catalysts pre-HDC

Catalyst	BET area ($m^2\ g^{-1}$)	TPR T_{max} (K)	H/Pd	H_2 uptake ($\mu mol\ g^{-1}$)	H_2 release ($\mu mol\ g^{-1}$)
Pd/SiO_2	191	**371**	0.34	6	7
La-Pd/SiO_2	156	**360**, 573	0.19	43	43
Ce-Pd/SiO_2	169	**364**, 573	0.21	43	41
Sm-Pd/SiO_2	164	**365**, 573	0.19	35	32
Eu-Pd/SiO_2	161	**365**, 537	0.18	47	49
Gd-Pd/SiO_2	162	**360**, 573	0.18	40	37
Yb-Pd/SiO_2	163	**361**, 544, 573	0.22	35	32

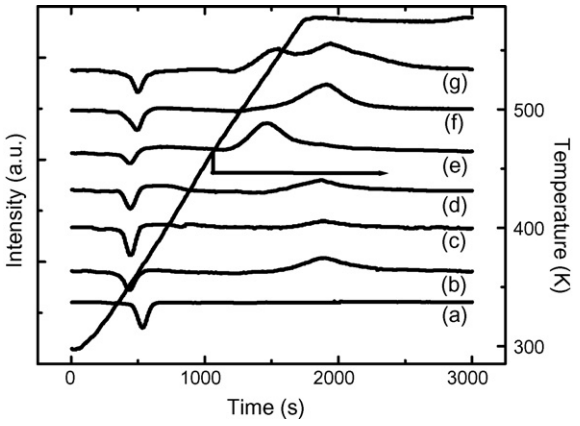

Fig. 1. TPR profiles of the passivated catalysts, pre-HDC: (a) Pd/SiO_2; (b) La-Pd/SiO_2; (c) Ce-Pd/SiO_2; (d) Sm-Pd/SiO_2; (e) Eu-Pd/SiO_2; (f) Gd-Pd/SiO_2; (g) Yb-Pd/SiO_2.

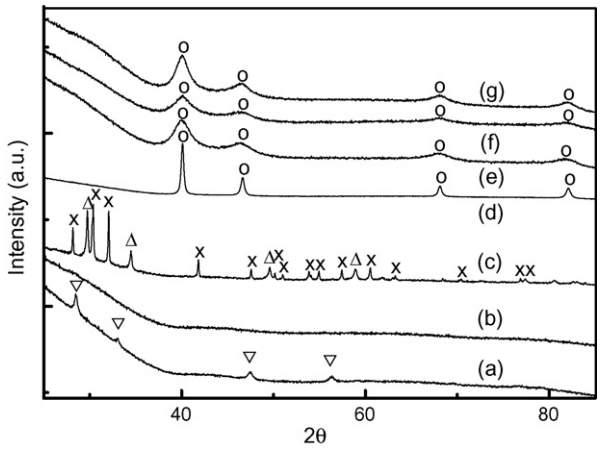

Fig. 2. XRD profiles recorded for the catalysts, pre-HDC: (a) Ce/SiO_2; (b) Eu/SiO_2; (c) Yb/SiO_2; (d) Pd/SiO_2; (e) Ce-Pd/SiO_2; (f) Eu-Pd/SiO_2; (g) Yb-Pd/SiO_2. Note O indicates peak assignment for Pd (fcc), X for YbH_2 (orthorhombic), △ for $Yb(NH_2)_x$ (bcc-tetragonal) and Yb_2O_3 (cubic) and ▽ for CeO_2 (cubic).

of the temperature ramp, suggesting a facile reduction of the passivated surface Pd. Indeed, room temperature reduction of PdO has been proposed in the literature [33,38,39]. The TPR profiles of the Ln/SiO_2 samples are not included in Fig. 1 as they were featureless without any measurable H_2 consumption or release (up to 573 K). It has been demonstrated elsewhere [40–43] that lanthanides can form hydrides (LnH_2/LnH_3) upon contact with H_2 at room temperature. Pd hydride exclusively adopts the α-form when H/Pd (mol ratio of H released to Pd_{total}, where $Pd_{total} = Pd_{surface} + Pd_{bulk}$) ≤ 0.01–0.03 and coexists in α- and β-phases for H/Pd up to 0.58–0.61 [44,45] where the β-form accounts for more than 95% of hydride with a limiting value of H/Pd in bulk Pd = 0.76 [46]. Higher apparent H/Pd ratios have been attributed to a trapping in and/or spillover of hydrogen onto the support [45]. The molar H/Pd ratios are presented in Table 1 where the value recorded for Pd/SiO_2 (0.34) is in accord with that reported in the literature [36,47] for related supported Pd systems. However, a greatly reduced H/Pd (0.20 ± 0.02) characterizes the bimetallic samples, suggesting that the presence of Ln inhibits Pd hydride formation.

XRD analysis was undertaken to probe bulk structural characteristics and the resultant diffractograms are presented in Fig. 2. The *d* spacings (2.24801, 1.94622, 1.37579, 1.17231, 1.12192, and 1.00515) associated with XRD pattern of Pd/SiO_2 are consistent with an exclusive cubic Pd symmetry [48]. Lanthanide metals dissolved in liquid NH_3, as is the case with our Ln/SiO_2 preparation, are known to form amines of the type $Ln(NH_2)_2/Ln(NH_2)_3$ [49]. The presence of YbH_2, $Yb(NH_2)_x$ and Yb_2O_3 [50] in Yb/SiO_2 is supported by XRD analysis (Profile (c) in Fig. 2) but as bcc-$Yb(NH_2)_2$ and cubic-Yb_2O_3 possess closely similar strong reflections, this has precluded an unambiguous decoupling/identification of the peaks. In contrast to Yb/SiO_2, Ce/SiO_2 did not exhibit any XRD reflections due to a hydride or amine but there is evidence for the presence of CeO_2; bulk ceria remains unreduced even up to 973 K [35]. The XRD profile for Eu/SiO_2 is featureless, suggesting a highly dispersed Eu phase. It should be noted that an XRD analysis of a 50%, w/w, Eu/SiO_2 sample did not reveal any reflections. The absence of an exclusive Ln phase is not unexpected as the generation of metallic Ln under atmospheric pressure requires a (carbothermal) reduction treatment at temperatures in excess of 2000 K [51]. The XRD profiles associated with the Ln-Pd/SiO_2 samples (representative profiles (e–g) in Fig. 2) only yielded reflections due to cubic Pd where the broad character of the Pd diffraction maxima suggests short range order; there was no evidence of bulk alloy formation.

While TPR of the passivated Pd/SiO_2 did not result in any detectable H_2 consumption, the bimetallic samples showed broad TPR H_2 consumption peaks over the *T* range 500–573 K (see Fig. 1). An exhaustive search through the published work did not reveal any directly comparable studies dealing with TPR analysis of supported Ln/Pd. Fígoli et al. [52] have, however, reported an increase in reduction temperature (from 367 to 403 K) with increasing La_2O_3 addition to Pd/SiO_2 and linked this response to a "blocking effect" by the lanthanide that hinders the reduction of PdO; they claim that La_2O_3 cannot be reduced in the *T* range 273–973 K. Yang et al. [53] have also reported an inhibited reduction of PdO supported on alumina due to the addition of La_2O_3 with a shift in T_{max} by up to 40 K from the value of 353 K that characterized reduction of PdO/γ-Al_2O_3. Weyrich et al. [35] have observed two reduction peaks (570 and 740 K) for CeO_2 in CeO_2/Na-ZSM5. As noted above, our XRD analysis of Ce/SiO_2 (exposed to a reductive atmosphere at 523 K) reveals the presence of CeO_2 that is not detectable for Ce-Pd/SiO_2. This observation can be attributed to a Pd promoted TPR of CeO_2 as has been proposed elsewhere [35]. It should be noted that TPR of Yb/SiO_2 (with a Yb_2O_3 component, see Fig. 2) to 1273 K [18] resulted in H_2 consumption at *ca*. 760 K attributed to oxide reduction. A Pd promoted oxide reduction may account, at least in part, for the H_2 consumption peaks that we have recorded for the passivated bimetallics. The possibility of surface Ln interactions that necessitate a higher PdO reduction temperature, while less likely in our pre-reduced/passivated samples particularly in the light of facile reduction of Pd/SiO_2, can not entirely be discounted.

3.1.2. TEM

TEM analysis of Pd/SiO_2 reported elsewhere [18,20] has shown that Pd is present as discrete particles with a pseudo-spherical morphology. The Ln/SiO_2 samples did not exhibit any comparable supported particles although EDX analysis demonstrated a significant lanthanide presence in all the areas that were mapped, suggesting a high dispersion; representative EDX results are given in Table 2a. The bimetallic catalysts exhibited an Ln content in excess of 0.3 atom% in every area that was analysed while Pd was again present as discrete particles. The Ln component is highly dispersed and in intimate contact with Pd; in those areas mapped that contained a significant Pd component, the Ln/Pd atomic ratios spanned the range 0.5–1.5. The surface weighted Pd particle sizes obtained from TEM are given in Table 2b where the values derived from XRD line broadening analysis are in reasonable agreement. The Pd particle size was significantly smaller in the bimetallics, a response that finds agreement in the work of Seoane et al. [22] who reported enhanced Pd dispersion as a result of La inclusion in silica supported Pd. A higher Pd dispersion in $Ln\text{-}Pd/SiO_2$ may contribute, in part, to the lower H/Pd ratios associated with Pd hydride. Nag et al. [36] observed a decrease in H/Pd ratio with increasing dispersion of Pd on carbon. A representative TEM image of a bimetallic catalyst ($Eu\text{-}Pd/SiO_2$) is shown in Fig. 3 where the encircled regions "a" and "b" correspond to Pd "rich" and Pd "lean" areas, respectively; the dashed circles are included to distinguish smaller Pd particles. From a consideration of the entries in Table 2a, it can be seen that while the Pd content in both mapped areas is quite different, the Eu content is similar, a response that is typical of the sample as a whole.

3.1.3. H_2 chemisorption/TPD

The H_2 uptake values for all the Pd-containing samples post-TPR are presented in Table 1. The Ln/SiO_2 samples exhibited low uptakes ($\leq 1\ \mu mol\ g^{-1}$) when compared with Pd/SiO_2. XRD analysis of Yb/SiO_2 (Fig. 2 profile (c)) established the presence of orthorhombic YbH_2 formed during TPR which accounts for limited uptake capacity in the subsequent room temperature H_2 pulse experiments. The same generic behavior should apply to all Ln/SiO_2, albeit there was no XRD detectable bulk hydride, presumably due to dispersion effects. The bimetallic samples exhibited H_2 uptakes that were up to eight times higher than that recorded for Pd/SiO_2 with the following sequence of increasing chemisorption: $Yb\text{-}Pd/SiO_2 \approx Sm\text{-}Pd/SiO_2 < Gd\text{-}Pd/SiO_2 < La\text{-}Pd/SiO_2 \approx Ce\text{-}Pd/SiO_2 < Eu\text{-}Pd/SiO_2$. An elevated H_2 uptake was also observed by Imamura et al. [23] during the hydrogenation of C_3H_4 over Yb promoted Pd/SiO_2 catalyst but this H_2 enrichment necessitated the presence of C_3H_4 and the same response was not observed with C_2H_2 addition. Seaone et al. [22] reported a higher H_2 uptake on a co-impregnated $La/Pd/SiO_2$ (after calcination/reduction) and attributed this effect to the formation of smaller Pd particles which also applies (see Table 2b) to our samples. Indeed, assuming dissociative adsorption on Pd (H:Pd stoichiometric ratio = 1), surface weighted Pd particle sizes obtained from H_2 chemisorption values [54] are included in Table 2b where again the bimetallic samples exhibit smaller Pd particles. It should, however, be noted that while the Pd particle sizes obtained from TEM and H_2 chemisorption analyses are in close agreement in the case of Pd/SiO_2, Pd particle sizes inferred

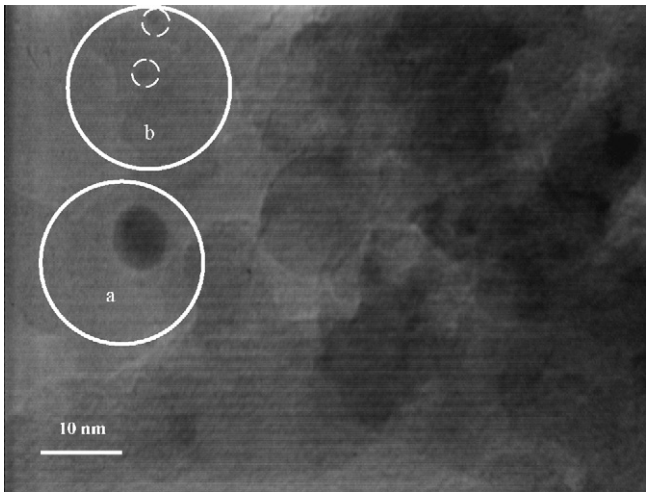

Fig. 3. Representative TEM image of $Eu\text{-}Pd/SiO_2$ pre-HDC. Note: elemental composition of areas "a" and "b" are given in Table 2a; dashed circles identify smaller Pd particles.

Table 2a
Representative elemental compositions based on EDX analysis of larger areas ($3 \times 10^5\ nm^2$) of selected Ln/SiO_2 samples and the regions labeled (a) and (b) in the TEM image of $Eu\text{-}Pd/SiO_2$ shown in Fig. 3

	EDX (atomic%)			
	Pd	Ln	Si	O
Eu/SiO_2	–	0.5	36.9	62.7
Yb/SiO_2	–	0.6	34.4	65.0
$Eu\text{-}Pd/SiO_2$ (a)	3.4	1.8	40.8	54.1
$Eu\text{-}Pd/SiO_2$ (b)	1.0	1.5	35.0	62.4

Table 2b
Average Pd particle sizes from H_2 chemisorption, TEM (surface weighted) and XRD analyses

	H_2 chemisorption (nm)		TEM (nm)		XRD (nm)	
	Unused	Used	Unused	Used	Unused	Used
Pd/SiO_2	40	71	36 (<2–50)[a]	48 (<5–76)[a]	33	42
$Ce\text{-}Pd/SiO_2$	5	6	11 (<2–20)	17 (<2–30)	7	9
$Eu\text{-}Pd/SiO_2$	5	6	13 (<2–20)	21 (<4–36)	8	11
$Yb\text{-}Pd/SiO_2$	6	7	7 (<2–15)	10 (<2–22)	–[b]	–[b]

[a] Pd particle size range.
[b] XRD peaks too broad for accurate Pd size measurement.

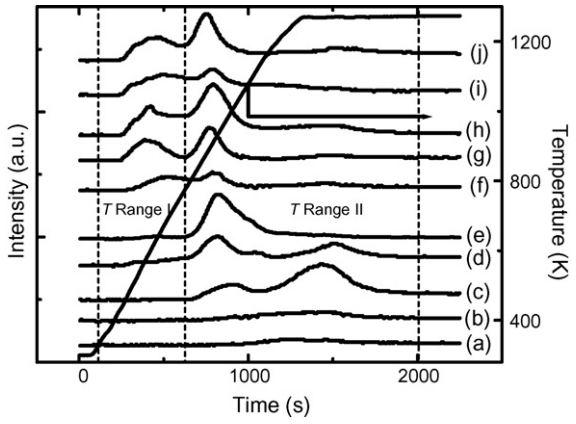

Fig. 4. H_2 TPD associated with: (a) Ce/SiO_2; (b) Eu/SiO_2; (c) Yb/SiO_2; (d) Pd/SiO_2; (e) $La\text{-}Pd/SiO_2$; (f) $Ce\text{-}Pd/SiO_2$; (g) $Sm\text{-}Pd/SiO_2$; (h) $Eu\text{-}Pd/SiO_2$; (i) $Gd\text{-}Pd/SiO_2$; (j) $Yb\text{-}Pd/SiO_2$, all pre-HDC.

from H_2 uptake were smaller than the TEM derived values for the bimetallic samples. Indeed, H_2 uptake on $Ln\text{-}Pd/SiO_2$ was higher (by a factor of up to 3) than that expected on the basis of the TEM analysis. Such a response suggests some surface interaction between Ln and Pd leading to higher H_2 uptake.

The TPD profiles (to 1273 K) following H_2 chemisorption are shown in Fig. 4. Each profile exhibits two regions of desorption, i.e. over the T range 500–750 K (Range I) and where $T > 750$ K (Range II). The desorption profiles for each Pd-containing sample were featureless at $T < 450$ K and the absence of a H_2 release peak at 360–370 K due to Pd hydride decomposition, observed during TPR (see Fig. 1), is consistent with an exclusive H_2 chemisorption during pulse titration, i.e. no hydride formation. TPD profiles generated for the Ln/SiO_2 samples were featureless where $T < 800$ K. Yb/SiO_2 demonstrated significant H_2 release over the T intervals 900–1050 K and 1150–1273 K with an ill-defined lesser H_2 desorption from Ce/SiO_2 and Eu/SiO_2. Imamura et al. have recorded TPD profiles for Yb/C [55] and Yb/MnO [49] where, in common with this study, Yb was introduced by impregnation from liquid NH_3. They reported low (<630 K) and high (>630 K) temperature peaks due to H_2 release (accompanied by NH_3 and N_2) as a result of the decomposition of $Yb(NH_2)_3/Yb(NH_2)_2$ with secondary H_2 release due to the decomposition of YbNH and YbH_2. The latter combined decomposition must give rise to the H_2 TPD response for Ln/SiO_2 recorded in this study. The reason for the lower intensity peaks generated by Ce/SiO_2 and Eu/SiO_2 relative to Yb/SiO_2 is not immediately obvious but may be due to differences in precursor decomposition during catalyst pre-treatment. A direct comparison of the H_2 TPD profiles generated in this study with the limited reports in the literature relating to supported Pd systems is problematic given the differences in metal loading/support/catalyst preparation/activation/desorption procedure. Sandoval et al. [56] have recorded three peaks in their H_2 TPD (415, 489, 550 K) from Pd/SiO_2 and attributed these to interaction with different Pd "sites" while Sepulveda et al. [57] observed removal of weakly held H_2 from Pd/SiO_2 at 273–500 K. The appearance of multiple TPD peaks has also been attributed to desorption of "re-adsorbed hydrogen" [57,58]. The quantity of H_2 released by the Pd and Pd/Ln systems over the T range I is recorded in Table 1 and essentially matches that taken up in the chemisorption step which preceded TPD. Hydrogen desorption over T range II is of comparable magnitude in each case, suggesting that H_2 release in T range II is largely insensitive to the nature of the Pd-Ln combination. Indeed, TPD response over this T range has been attributed elsewhere [32,59,60] to spillover H_2 release. We should also recognise a possible contribution due to the decomposition of LnH_2/LnH_3 [55] and the dehydroxylation of SiO_2, known to occur at elevated temperatures [61,62], to the overall TPD profile. The higher uptake

Table 3a
Pd, Ce, Eu, Yb and Cl binding energies (eV) and atomic (at.) ratios from XPS analysis of the catalysts pre- and post-HDC

	Pre-HDC				Post-HDC							
	Binding energy			Atomic ratio	Binding energy					Atomic ratio		
	Pd $3d_{5/2}$	Ln $d_{5/2}$		Ln/Pd	Pd $3d_{5/2}$		Ln $d_{5/2}$		Cl $2p_{3/2}$	Ln/Pd	Cl/Pd	Cl/(Ln + Pd)
Pd/SiO_2	334.3	–		–	334.3		–		–	–	–	–
Ce/SiO_2	–	**880.7**	885.7	–	–		–		–	–	–	–
Eu/SiO_2	–	1124.0	**1133.7**	–	–		–		–	–	–	–
Yb/SiO_2	–	**184.7**	–	–	–		–		–	–	–	–
$Ce\text{-}Pd/SiO_2$	334.4	880.9	**884.7**	1.1	334.7	336.6	881.1	**885.0**	197.6	0.7	1.9	1.1
$Eu\text{-}Pd/SiO_2$	334.4	1123.9	**1133.9**	1.7	335.0	336.9	1124.2	**1134.2**	197.7	2.0	2.1	0.7
$Yb\text{-}Pd/SiO_2$	334.3	**184.8**	–	0.5	334.4	336.7	**185.2**	–	197.7	0.8	4.2	2.3

Note: The binding energy for the major Ln peak is given in bold.

Table 3b
Pd, Yb and Cl binding energies (eV) and atomic ratios for model samples

	Binding energy (eV)			Atomic ratio		
	Pd $3d_{5/2}$	Yb $4d_{5/2}$	Cl $2p_{3/2}$	Yb/Pd	Cl/Pd	Cl/Yb
$PdCl_2 + SiO_2$	334.4, 336.2	–	196.9	–	1.6	–
$YbCl_3 + SiO_2$	–	185.2	197.3	–	–	3.3

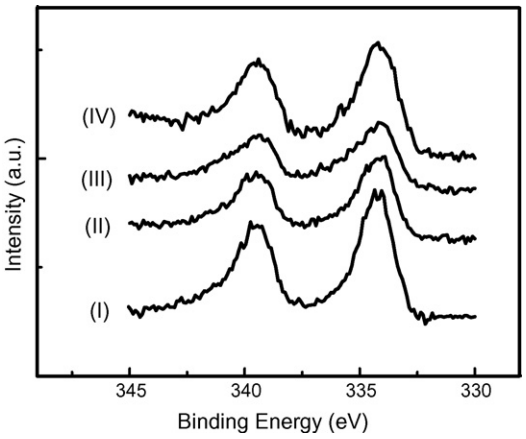

Fig. 5. XPS spectra over the Pd 3d region recorded for: (I) Pd/SiO_2; (II) Ce-Pd/SiO_2; (III) Eu-Pd/SiO_2; (IV) Yb-Pd/SiO_2, all pre-HDC.

and associated H_2 release that characterizes Ln-Pd/SiO_2 will be shown to have significant implications for catalytic activity.

3.1.4. XPS

XPS spectra of the passivated samples over the Pd and Ln (Ce, Eu and Yb) binding energy regions are presented in Figs. 5 and 6; the associated binding energies and surface compositions are given in Table 3a. The XPS spectrum generated for Pd/SiO_2 (profile (I) in Fig. 5) exhibits two peaks where the associated Pd $3d_{5/2}$ binding energy is in good agreement with that recorded in the literature [22,35]. There was no detectable shift in Pd $3d_{5/2}$ binding energy for the Ln-Pd/SiO_2 samples relative to Pd/SiO_2, which suggests that electron transfer from electropositive Ln to Pd as has been suggested elsewhere [22] is not a feature of our systems. Monometallic Ce/SiO_2 and Eu/SiO_2 were characterized by two $3d_{5/2}$ peaks (one dominant peak with a secondary peak or shoulder) while Yb/SiO_2 exhibited only one $4d_{5/2}$ peak. The Yb $4d_{5/2}$ binding energies recorded for the Yb/SiO_2 and Yb-Pd/SiO_2 samples pre-HDC (Table 3a) are close to that reported in the literature [63] for Yb^{3+} (185 eV for Yb_2O_3). The binding energy associated with the principal XPS signal for Ce/SiO_2 is similar to that recorded for CeO_2 (881.5 eV) while the secondary peak at higher binding energy can be linked to Ce_2O_3 (885.1 eV) [64,65]. It is instructive to note that the peak dominance is switched in the bimetallic sample where the signal due to Ce_2O_3 is stronger, suggesting partial surface reduction due to the presence of Pd as inferred from the TPR results. The higher binding energy signal recorded for Eu/SiO_2 is in excellent agreement with that assigned to Eu_2O_3 (1133.7 eV) [66] and the lower binding energy (for the less intense peak) may be attributed to Eu metal (1125.4 eV) in line with the work of Cai et al. [67]. The range of Ln/Pd surface atomic ratios (0.5–1.7) in the unused sample spanned the bulk ratio (0.7) and is similar to that observed in the TEM–EDX analysis (0.5–1.5); there appears to be a significant surface enrichment by Eu.

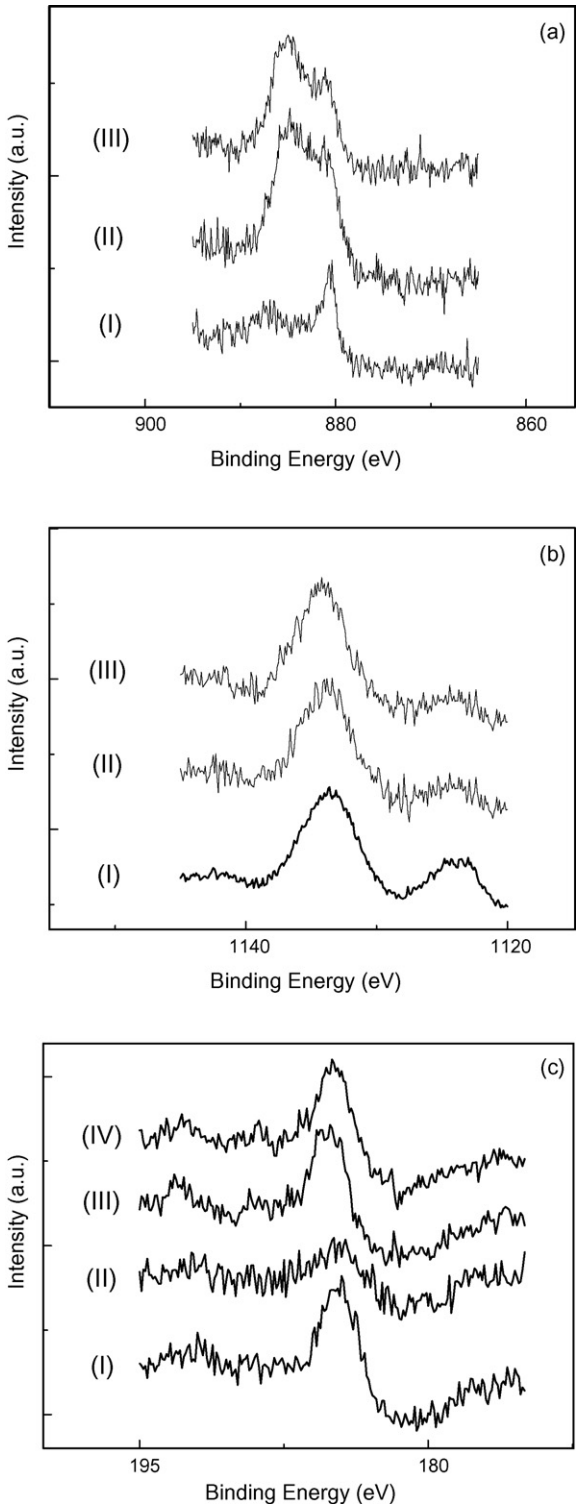

Fig. 6. (a) XPS spectra over the Ce 3d region recorded for: (I) Ce/SiO_2, pre-HDC; (II) Ce-Pd/SiO_2, pre-HDC; (III) Ce-Pd/SiO_2, post-HDC. (b) XPS spectra over the Eu 3d region for: (I) Eu/SiO_2, pre-HDC; (II) Eu-Pd/SiO_2, pre-HDC; (III) Eu-Pd/SiO_2, post-HDC. (c) XPS spectra over the Yb 4d region for: (I) Yb/SiO_2, pre-HDC; (II) Yb-Pd/SiO_2, pre-HDC; (III) Yb-Pd/SiO_2, post-HDC; (IV) $YbCl_3 + SiO_2$.

3.2. HDC activity/selectivity

HDC of CB over Pd/SiO_2 and Ln-Pd/SiO_2 generated benzene as the predominant product with trace amounts of cyclohex-

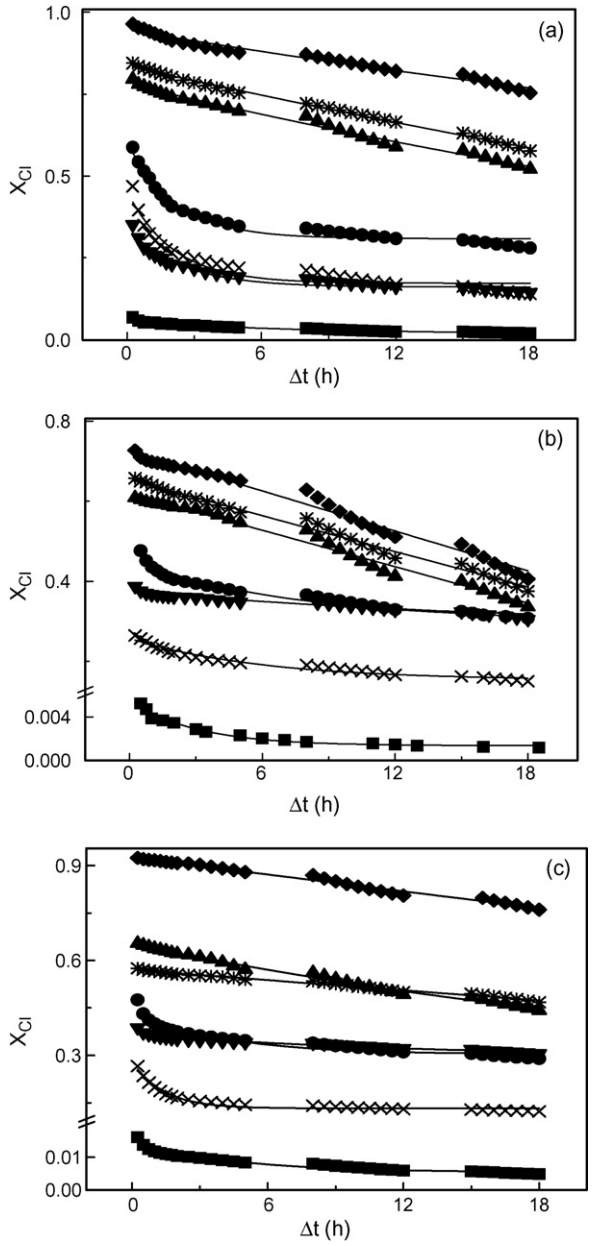

Fig. 7. Fractional dechlorination (x_{Cl}) of: (a) CB; (b) 1,2-DCB; (c) 1,3-DCB as a function of time-on-stream over Pd/SiO_2 (■), La-Pd/SiO_2 (▲), Ce-Pd/SiO_2 (✱), Sm-Pd/SiO_2 (▼), Eu-Pd/SiO_2 (◊), Gd-Pd/SiO_2 (●) and Yb-Pd/SiO_2 (×): inlet hourly Cl/Pd mole ratio = 5×10^3; $T = 423$ K. *Note:* lines represent fits to Eq. (4).

ane (<1% conversion) while conversion of DCB also yielded CB as a partially dechlorinated product, reaction trends that find agreement elsewhere [8,17,68,69]. Time-on-stream activity plots for the conversion of CB, 1,2-DCB and 1,3-DCB are shown in Fig. 7; HDC over Ln/SiO_2 resulted in a negligible (<0.1%) conversion. The catalytic data were fitted using the empirical exponential decay Eq. (4) and the fits are included in Fig. 7. Fit convergence yielded values for x_0, the initial fractional HDC, which are included in Table 4. It is immediately evident that Ln served as an effective HDC promoter with the following activity sequence based on initial CB conversion: Pd/SiO_2 < Sm-Pd/SiO_2 < Yb-Pd/SiO_2 < Gd-Pd/SiO_2 < La-Pd/SiO_2 < Ce-Pd/SiO_2 < Eu-Pd/SiO_2. A similar order of increasing HDC activity holds for the conversion of both DCB reactants with the exception that Sm-Pd/SiO_2 outperformed Yb-Pd/SiO_2 and the fractional dechlorination converged for La-Pd/SiO_2 and Ce-Pd/SiO_2. The presence of Ln resulted in an increase in HDC performance by up to two orders of magnitude as can be assessed from Fig. 8 where initial specific activity increased from the lowest value (0.01 $mol_{Cl}\ mol_{Pd}\ s^{-1}$) for Pd/SiO_2 to the highest value (1.3 $mol_{Cl}\ mol_{Pd}\ s^{-1}$) for Eu-$Pd/SiO_2$. Each catalyst exhibited a temporal drop in activity irrespective of the feed. It is, however, significant that the Ln-Pd/SiO_2 systems maintained a higher fractional dechlorination in every instance and were more resistant to deactivation as can be assessed from the ratio of final to initial fractional dechlorination, i.e. the $x_{18\,h}/x_0$ entries in Table 4. Fractional dechlorination of DCB was lower than that recorded for CB (at a common inlet Cl/Pd), which is consistent with reports in the literature [70–73] that gas phase haloarene hydrodehalogenation proceeds *via* an electrophilic mechanism involving a delocalized carbocation (arenium ion) intermediate as the transition complex in the rate determining step; the presence of the second electron withdrawing Cl substituent has a deactivating effect that serves to lower reactivity.

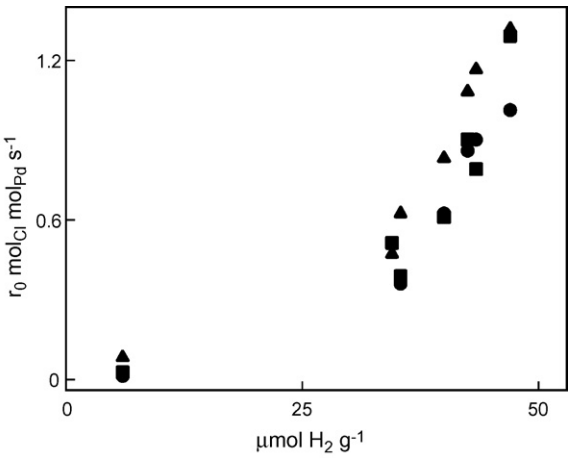

Fig. 8. Initial CB (▲), 1,2-DCB (●) and 1,3-DCB (■) HDC rates (r_0) as a function of H_2 uptake: inlet hourly Cl/Pd mole ratio = 5×10^3; $T = 423$ K.

The initial HDC rates increased with increasing H_2 chemisorption, as illustrated in Fig. 8, where the enhanced H_2 uptake/release characteristics associated with Ln-Pd/SiO_2 translates into intrinsically more effective catalytic HDC performance. Such an observation finds support in the contention of Estellé et al. [74] that HDC rates depend more on H_2 adsorption/desorption behavior than on the nature of the haloarene reactant. A comparison of the initial HDC specific rates (R_0, per unit surface area based on TEM measurements, see Table 4) suggests that Ln-Pd/SiO_2 with smaller Pd particles (mean < 13 nm, see Table 2b) were significantly more active compared with Pd/SiO_2 (36 nm). This observation is in contrast to published studies [15,16] where a higher HDC turnover frequency was associated with larger supported metal particles and attributed to an ensemble effect. In this study, the contribution due to a surface Pd-Ln synergism leading to higher associated levels

Table 4
Initial fractional dechlorination (x_0) of CB, 1,2-DCB and 1,3-DCB, ratio of final ($x_{18\,h}$, after 18 h on-stream) to initial HDC activity, initial selectivity to benzene ($S_{benzene}$%) in the conversion of both DCB isomers and initial specific dechlorination rate (R_0, units: 10^{-2} mol_{Cl} h^{-1} m^{-2}): inlet hourly Cl/Pd mole ratio = 5×10^3; T = 423 K

	Pd/SiO_2	$La\text{-}Pd/SiO_2$	$Ce\text{-}Pd/SiO_2$	$Sm\text{-}Pd/SiO_2$	$Eu\text{-}Pd/SiO_2$	$Gd\text{-}Pd/SiO_2$	$Yb\text{-}Pd/SiO_2$
CB feed							
x_o	0.06	0.78	0.84	0.38	0.95	0.60	0.45
$x_{18\,h}/x_0$	0.27	0.67	0.68	0.42	0.80	0.47	0.33
R_0	24	–	87	–	117	–	51
1,2-DCB feed							
x_o	0.01	0.62	0.65	0.34	0.73	0.45	0.26
$x_{18\,h}/x_0$	0.22	0.55	0.59	0.79	0.55	0.69	0.59
$S_{benzene}$ (%)	19	89	94	87	94	88	80
R_0	4	–	68	–	90	–	30
1,3-DCB feed							
x_0	0.02	0.65	0.57	0.34	0.92	0.44	0.28
$x_{18\,h}/x_0$	0.21	0.68	0.81	0.79	0.82	0.66	0.45
$S_{benzene}$ (%)	0	85	82	73	97	80	71
R_0	8	–	59	–	114	–	32

of surface reactive hydrogen with a commensurate increase in HDC rate must surpass any possible ensemble effect. Taking an overview of the range of supported Pd-lanthanide catalysts, which possess a comparable mean Pd size (and size range), it is significant that the highest specific HDC rates were delivered by $Eu\text{-}Pd/SiO_2$ which exhibited higher surface Ln/Pd atomic ratios (from TEM/XPS analysis). While the XPS results (see Table 3a) discount any significant electron transfer from Ln to Pd, Ln electronic structure may well have a bearing on chloroarene activation, influencing hydride reactivity and Cl/surface interactions. The latter is a definite consideration given the affinity of Ln to form Ln chlorides [40,50]. Three factors can impact on the promotional Ln influence in terms of Pd HDC performance: (i) atomic radius; (ii) ionization energy (IE); (iii) heat of formation of LnH_2. The sequence of HDC activity among the $Ln\text{-}Pd/SiO_2$ samples can be associated with the general periodic trend across the group where the larger radius lanthanides generally exhibit greater reactivity [40], which can impact on C–Cl bond activation. A lower IE or higher electropositivity should result in enhanced C–Cl bond activation where the reference [75] IE value for La, Ce, Sm and Eu (5.6 eV) is less than that (6.2 eV) which characterizes Gd and Yb. The heat of Ln hydride formation is equivalent to the dissociation energy, $LnH_2 \rightarrow Ln + 2H$ and can serve as a measure of atomic hydrogen transfer. Ionov and Kuznetsov have recorded [76] exothermic standard heats of formation (ΔH_f) for La, Ce, Eu and Yb in the range 208–218 kJ mol^{-1} while the values for Gd and Sm are 204 and 224 kJ mol^{-1}, respectively. With a view to correlating Ln electronic structure and LnH_2 stability with the HDC activity data recorded in Table 4, the most active bimetallic ($Eu\text{-}Pd/SiO_2$) contains an Ln promoter with a half filled 4f orbital, the largest atomic radius (208.4 pm) of all the lanthanides and lower IE, which we tentatively link to enhanced C–Cl bond activation and/or hydrogen transfer. The least active bimetallic ($Yb\text{-}Pd/SiO_2$) contains Ln with the second largest atomic size (193.3 pm) but possessing a completely filled 4f valence shell and an associated stability that results in a lesser contribution to HDC activity. In crossing the Periodic Table (from La to Yb), the high and comparable HDC activity delivered by $Ce\text{-}Pd/SiO_2$ and $La\text{-}Pd/SiO_2$ can be related to larger atomic radii (182 and 187 pm, respectively) and an associated lower IE that facilitates an activation of C–Cl bond(s) due to the relative ease of electron donation. The intermediate HDC performance delivered by the incorporation of Gd (180.4 pm) can be linked to a favorable low ΔH_f (LnH_2) that is however compensated somewhat by a higher IE while the higher ΔH_f (LnH_2) associated with Sm (180.4 pm) contributes to the lower activity generated by $Sm\text{-}Pd/SiO_2$ as a result of a less effective hydrogen transfer. The enhanced HDC performance of the $Ln\text{-}Pd/SiO_2$ samples is perhaps best illustrated in Fig. 9 where benzene selectivity (complete HDC) is plotted as a function of fractional DCB conversion (x_{DCB}). The degree of complete HDC over $Ln\text{-}Pd/SiO_2$ is such that there is no possible overlap with the selectivity profile generated for

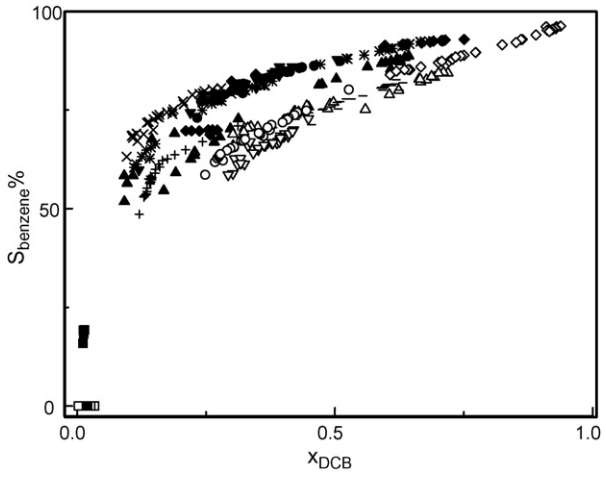

Fig. 9. Benzene selectivity ($S_{benzene}$%) as a function of fractional 1,2-DCB (solid symbols, ✱ and ×) and *1,3*-DCB (open symbols, − and +) for HDC over Pd/SiO_2 (■,□), $La\text{-}Pd/SiO_2$ (▲,△), $Ce\text{-}Pd/SiO_2$ (✱, −), $Sm\text{-}Pd/SiO_2$ (▼,▽), $Eu\text{-}Pd/SiO_2$ (♦,◊), $Gd\text{-}Pd/SiO_2$ (●,○) and $Yb\text{-}Pd/SiO_2$ (×,+): inlet hourly Cl/Pd mole ratio = 5×10^3; T = 423 K.

Table 5
BET surface area, H_2 uptake and corresponding H_2 release (over T range I identified in Fig. 4) associated with catalysts post-HDC: inlet hourly Cl/Pd mole ratio = 5×10^3; T = 423 K

Catalyst	BET area ($m^2\,g^{-1}$)	H_2 uptake ($\mu mol\,g^{-1}$)	H_2 release ($\mu mol\,g^{-1}$)
Pd/SiO_2	184	2	<1
Ce-Pd/SiO_2	155	38	36
Eu-Pd/SiO_2	154	41	40
Yb-Pd/SiO_2	153	32	30

Pd/SiO_2. Moreover, the $S_{benzene}$ values at a given x_{DCB} are consistently higher for 1,2-DCB, suggesting the preferred removal of both Cl sustituents from the *ortho*-isomer.

3.3. Catalyst characterization: post-HDC

All the catalysts studied exhibited a loss of activity with time-on-stream, a response that has been attributed in other HDC applications to poisoning by HCl [8,15,77,78], coking [78] and metal sintering [8]. The BET areas of the spent catalysts were uniformly lower than those recorded pre-HDC but the difference (see Table 5) was not appreciable. The TPR profiles of the samples post-HDC (see Fig. 10 for four representative cases) are again dominated by a negative peak due to Pd hydride decomposition. It is, however, noteworthy that the peak position is shifted slightly to a higher temperature (370 ± 5 K), a response that has been attributed elsewhere [36,47] to an increase in Pd particle size where the hydride is more strongly held in the metal lattice. Hydrogen uptake on the used Pd/SiO_2 was significantly lower (see Table 5), an effect that suggests a decrease in the metal dispersion; metal agglomeration during HDC has been noted elsewhere [5,8,79]. Indeed, the entries in Table 2b reveal a general shift in Pd particle size to larger values post-HDC. Hydrogen uptake on the Ln-Pd/SiO_2 samples was slightly lower post-HDC. The TPD profiles (not shown) did not deviate significantly from those generated for the unused samples (see Fig. 4) and H_2 release (where T = 500–750 K) was again close to that adsorbed in the chemisorption step; see Table 5.

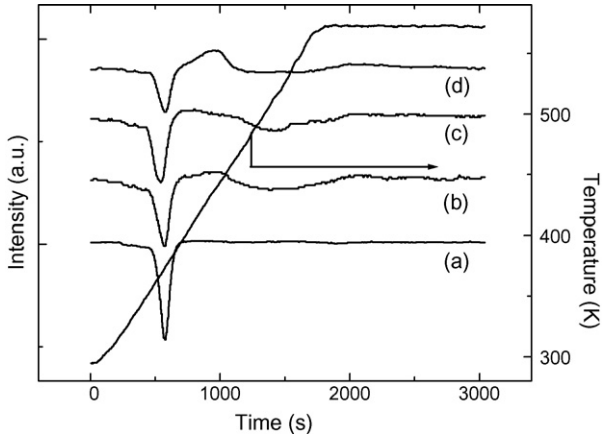

Fig. 10. TPR profiles of the passivated catalysts post-HDC: (a) Pd/SiO_2 (H/Pd = 0.59); (b) Ce-Pd/SiO_2 (H/Pd = 0.27); (c) Eu-Pd/SiO_2 (H/Pd = 0.23); (d) Yb-Pd/SiO_2 (H/Pd = 0.21).

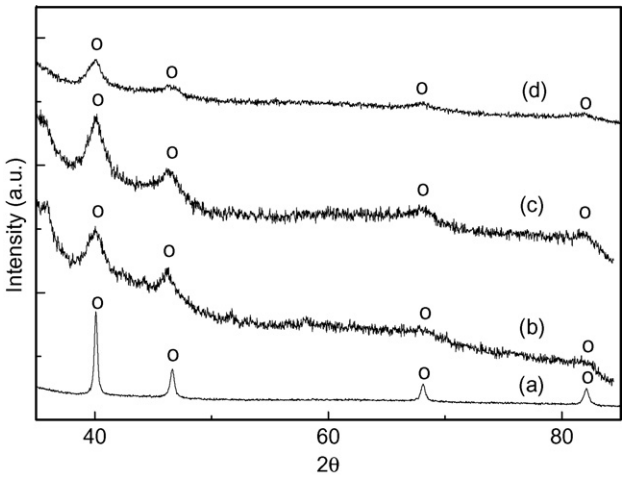

Fig. 11. XRD of the catalysts post-HDC: (a) Pd/SiO_2; (b) Ce-Pd/SiO_2; (c) Eu-Pd/SiO_2; (d) Yb-Pd/SiO_2. *Note:* O indicates peak assignment for Pd (fcc).

Structural change to the Pd/SiO_2 sample during HDC is evident in the appreciably higher H/Pd ratio associated with Pd hydride decomposition (see caption to Fig. 10) during TPR, an effect that has been linked elsewhere to metal sintering [36,47]. The occurrence of positive TPR peaks for the three used Ln-Pd/SiO_2 samples (T > 400 K) may be due to H_2 consumption due to reaction with surface chloride but this was not a feature of the TPR of Pd/SiO_2 post-HDC. Indeed, passage of the effluent gas during TPR of the used bimetallics through an aqueous NaOH trap ($3.5–8.0 \times 10^{-3}$ mol dm^{-3}, agitation at 400 rpm, continuous pH data logging [80]) revealed a drop in pH that is consistent with HCl release. However, there was no evidence for the incorporation of Cl in the bulk catalyst structure, on the basis of the XRD profiles presented in Fig. 11 where the signals are due solely to a cubic Pd phase. The presence of surface Cl in post-HDC bimetallic samples is confirmed from XPS analysis, as shown in Fig. 12(a) with the emergence of a Cl 2p signal. There was no detectable surface Cl in the post-HDC Pd/SiO_2 sample and the XPS spectrum over the Pd 3d region (Fig. 12(b)) is indistinguishable from that recorded for the sample pre-HDC (Fig. 5), characterized by distinct Pd $3d_{3/2}$ and Pd $3d_{5/2}$ signals with identical binding energies (Table 3a). The XPS Pd profiles recorded for the Ln-Pd/SiO_2 samples have clearly been disrupted as a result of HDC with a splitting of the Pd $3d_{3/2}$ and $3d_{5/2}$ signals, a feature that is characteristic of the XPS spectra of $PdCl_2$, which is also included (physical mixture with SiO_2) in Fig. 12. The binding energies for both Pd $3d_{5/2}$ peaks associated with $PdCl_2 + SiO_2$ (Table 3b) match those recorded for the three bimetallic catalysts post HDC and are consistent with Pd^{2+} [77]. It should be noted that the principal Ln $3d_{5/2}$ (or $4d_{5/2}$) peak was shifted by up to 0.4 eV to approach that of $LnCl_3$; see entries in Tables 3a and 3b. In terms of atomic ratios, the post-HDC bimetallics exhibit a surface saturation by Cl (Table 3a) which is in keeping with strong Cl/Ln interaction(s). This residual surface Cl may contribute to the observed temporal decline, albeit far less severe than that observed for Pd/SiO_2, in HDC performance through interference in chloroarene activation. Moreover, it is known

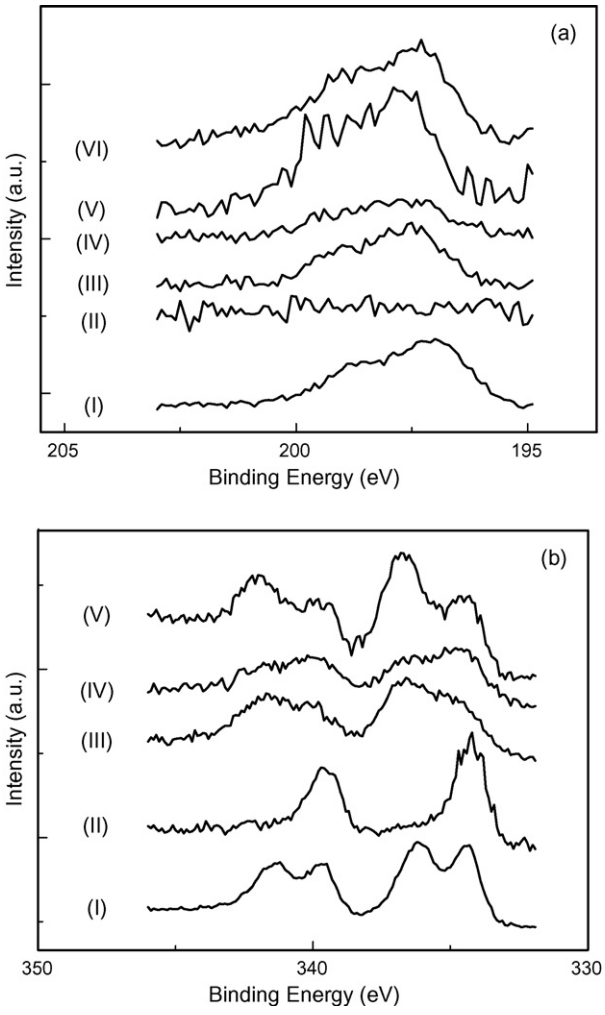

Fig. 12. (a) XPS spectra over the Cl 2p region for: (I) $PdCl_2 + SiO_2$; (II) Pd/SiO_2, post-HDC; (III) Ce-Pd/SiO_2, post-HDC; (IV) Eu-Pd/SiO_2, post-HDC; (V) Yb-Pd/SiO_2, post-HDC; (VI) $YbCl_3 + SiO_2$. (b) XPS spectra over the Pd 3d region for: (I) $PdCl_2 + SiO_2$; (II) Pd/SiO_2, post-HDC; (III) Ce-Pd/SiO_2, post-HDC; (IV) Eu-Pd/SiO_2, post-HDC; (V) Yb-Pd/SiO_2, post-HDC.

[18] that Cl can have a deleterious effect on Ln hydride formation.

4. Conclusions

In the gas phase HDC of CB, 1,2-DCB and 1,3-DCB over Pd/SiO_2 and Ln-Pd/SiO_2 (Ln = La, Ce, Sm, Eu, Gd and Yb), the inclusion of Ln (*via* the $\{(DMF)_{10}Ln_2[Pd(CN)_4]_3\}_\infty$ precursor) served to promote HDC performance by up to two orders of magnitude. Moreover, the Ln-Pd/SiO_2 catalysts maintained a higher degree of their initial activity with increasing time-on-stream. While Ln/SiO_2 exhibited negligible dechlorination activity, a surface Ln/Pd synergism delivered the following overall sequence of increasing initial fractional dechlorination: $Pd/SiO_2 < Yb\text{-}Pd/SiO_2 \approx Sm\text{-}Pd/SiO_2 < Gd\text{-}Pd/SiO_2 < La\text{-}Pd/SiO_2 \approx Ce\text{-}Pd/SiO_2 < Eu\text{-}Pd/SiO_2$. The Ln-$Pd/SiO_2$ system is characterized by appreciably smaller Pd particles where the Ln component is present as a finely dispersed phase. TPR of the bimetallic samples generated a negative (H_2 release) peak due to Pd hydride decomposition where Ln inhibited Pd hydride formation. Hydrogen chemisorption measurements revealed a significant enhancement of H_2 uptake on Ln-Pd/SiO_2 that was matched by the H_2 TPD response and suggests a Pd/Ln synergism that serves to generate a higher surface hydrogen content. The initial HDC rates correlate with H_2 uptake values while the Ln component may contribute directly to activation of the C-Cl bond(s) for hydrogenolytic attack. The latter possibility is supported by the high Cl content (from XPS analysis) of the Ln-Pd/SiO_2 samples post-HDC that was not a feature of Pd/SiO_2.

Acknowledgements

This work was supported in part by the National Science Foundation through Grant CTS-0218591 which MAK acknowledges. SGS also thanks the National Science Foundation for support through Grants CHE-9901115 and CHE-0213491.

References

[1] J.K. Fawell, S. Hunt, Environmental Toxicology, Organic Pollutants, Ellis Horwood, Chichester, 1988.
[2] E. Goldberg, Sci. Total Environ. 100 (1991) 17.
[3] Environmental Protection Agency, The Inventory of Sources of Dioxin in the United States, EPA/600/P-98/002, 1998.
[4] Environmental Protection Agency, OPPT Chemical Fact Sheets, Pollution Prevention and Toxics (7407), EPA 749-F-95-007a, Support Document: CAS No. 108-90-7, 1995.
[5] M.A. Keane, in: M.A. Keane (Ed.), Interfacial Applications in Environmental Engineering, Marcel Dekker, New York, 2002, pp. 231–254.
[6] F.J. Urbano, J.M. Marinas, J. Mol. Catal. A: Chem. 173 (2001) 329.
[7] B. Coq, G. Ferrat, F. Figueras, J. Catal. 101 (1986) 434.
[8] A. Gampine, D.P. Eyman, J. Catal. 179 (1998) 315.
[9] N. Lingaiah, P.S.S. Prasad, P.K. Rao, L.E. Smart, F.J. Berry, Appl. Catal. A: Gen. 213 (2001) 189.
[10] K.V. Murthy, P.M. Patterson, G. Jacobs, B.H. Davis, M.A. Keane, J. Catal. 223 (2004) 74.
[11] K.V. Murthy, P.M. Patterson, M.A. Keane, J. Mol. Catal. A: Chem. 225 (2005) 149.
[12] E. Lopez, S. Ordonez, H. Sastre, F.V. Diez, J. Hazard. Mater. 97 (2003) 281.
[13] F. Alonso, I.P. Beletskaya, M. Yus, Chem. Rev. 102 (2002) 4009.
[14] S.B. Halligudi, B.M. Devassay, A. Ghosh, V. Ravikumar, J. Mol. Catal. A: Chem. 184 (2002) 175.
[15] R. Gopinath, K.N. Rao, P.S.S. Prasad, S.S. Madhavendra, S. Narayanan, G. Vivekanandan, J. Mol. Catal. A: Chem. 181 (2002) 215.
[16] W. Juszczyk, A. Malinowski, Z. Karpiński, Appl. Catal. A: Gen. 166 (1998) 311.
[17] S. Jujjuri, E. Ding, S.G. Shore, M.A. Keane, Appl. Organomet. Chem. 17 (2003) 493.
[18] S. Jujjuri, E. Ding, E.L. Hommel, S.G. Shore, M.A. Keane, J. Catal. 239 (2006) 486.
[19] S.G. Shore, E. Ding, C. Park, M.A. Keane, Catal. Commun. 3 (2002) 77.
[20] S.G. Shore, E. Ding, C. Park, M.A. Keane, J. Mol. Catal. A: Chem. 212 (2004) 291.
[21] T. Teranishi, K. Nakata, M. Iwamoto, M. Miyake, N. Toshima, React. Funct. Polym. 37 (1998) 111.
[22] X.L. Seoane, N.S. Fígoli, P.C.L. Argentiere, J.A. González, A. Arcoya, Catal. Lett. 47 (1997) 213.
[23] H. Imamura, M. Suzuki, Y. Sakata, S. Tsuchiya, J. Alloys Compd. 303–304 (2000) 514.
[24] R. Wang, C. Lin, T. Chen, J. Lin, S. Mao, Cuihua Xuebao 25 (2004) 711.
[25] S. Coman, F. Vasiliu, V. Parvulescu, Rev. Roamaine Chim. 47 (2002) 353.

[26] V. Parvulescu, E. Angelescu, I.V. Nicolescu, Rev. Roamaine Chim. 37 (1992) 453.
[27] Z. Xie, C. Qian, Y. Huang, J. Organomet. Chem. 412 (1991) 61.
[28] C. Qian, G. Zou, L. Gao, J. Organomet. Chem. 525 (1996) 23.
[29] D.W. Knoeppel, J. Liu, E.A. Meyers, S.G. Shore, Inorg. Chem. 37 (1998) 4828.
[30] E.-J. Shin, M.A. Keane, J. Chem. Technol. Biotechnol. 75 (2000) 159.
[31] M.A. Keane, D.Y. Murzin, Chem. Eng. Sci. 56 (2001) 3185.
[32] E.-J. Shin, A. Spiller, G. Tavoularis, M.A. Keane, Phys. Chem. Chem. Phys. 1 (1999) 3173.
[33] C.-B. Wang, H.-K. Lin, C.-M. Ho, J. Mol. Catal A: Chem. 180 (2002) 285.
[34] F.B. Noronha, M. Schmal, B. Moraweck, P. Delichère, M. Brun, F. Villain, R. Fréty, J. Phys. Chem. B 104 (2000) 5478.
[35] P.A. Weyrich, H. Treviño, W.F. Hölderich, W.M.H. Sachtler, Appl. Catal. A: Gen. 163 (1997) 31.
[36] N.K. Nag, J. Phys. Chem. B 105 (2001) 5945.
[37] W. Juszczyk, Z. Karpiński, D. Łomot, J. Pielaszek, Z. Paál, A.Y. Stakheev, J. Catal. 142 (1993) 617.
[38] G.M. Tonetto, D.E. Damiani, J. Mol. Catal. A: Chem. 202 (2003) 289.
[39] F. Pinna, F. Menegazzo, M. Signoretto, P. Canton, G. Fagherazzi, N. Pernicone, Appl. Catal. A: Gen. 219 (2001) 195.
[40] N.N. Greenwood, A. Earnshaw, Chemistry of the Elements, second ed., Butterworth-Heinemann, Oxford, 1998.
[41] V.M. Kuz'menko, A.N. Vladychkin, Phys. Solid State Met. Supercond. 41 (1999) 155.
[42] A.E. Curzon, O. Singh, J. Phys. D: Appl. Phys. 8 (1975) 1703.
[43] A.E. Curzon, O. Singh, J. Less Common Met. 39 (1975) 227.
[44] A.D. Ninno, V. Violante, A.L. Barbera, Phys. Rev. B 56 (1997) 2417.
[45] A. Rose, S. Maniguet, R.J. Mathew, C. Slater, J. Yao, A.E. Russell, Phys. Chem. Chem. Phys. 5 (2003) 3220.
[46] N. Nishimiya, T. Kishi, T. Mizushima, A. Matsumoto, K. Tsutsumi, J. Alloys Compd. 319 (2001) 312.
[47] F. Pinna, M. Signoretto, G. Strukul, S. Polizzi, N. Pernicone, React. Kinet. Catal. Lett. 60 (1997) 9.
[48] A. Kern, W. Eysel, Mineralogisch Petrograph, Univ. Heidelberg, 1983; CAS: 7440-05-3.
[49] H. Imamura, K. Nishimura, T. Yoshimura, H. Yoshimochi, M. Ueno, Y. Sakata, S. Tsuchiya, J. Mol. Catal. A: Chem. 165 (2001) 189.
[50] S. Cotton, Lanthanides and Actinides, Oxford University Press, New York, 1991, p. 17.
[51] J.C. Achard, C.N.R.S. Meudon-Bellevue, Rev. Intern. Hautes Temp. Refract. 3 (1966) 281.
[52] N.S. Fígoli, P.C. L'Argentiere, A. Arcoya, X.L. Seoane, J. Catal. 155 (1995) 95.
[53] C. Yang, J. Ren, Y. Sun, Catal. Lett. 84 (2002) 123.
[54] R.J. Matyi, L.H. Schwartz, J.B. Butt, Catal. Rev. Sci. Eng. 29 (1987) 41.
[55] H. Imamura, Y. Maeda, T. Kumai, Y. Sakata, S. Tsuchiya, Catal. Lett. 88 (2003) 69.
[56] V.H. Sandoval, C.E. Gigola, Appl. Catal. A: Gen. 148 (1996) 81.
[57] J.H. Sepúlveda, N.S. Fígoli, Appl. Surf. Sci. 68 (1993) 257.
[58] J.S. Rieck, A.T. Bell, J. Catal. 85 (1984) 143.
[59] F. Benseradj, F. Sadi, M. Chater, Appl. Catal. A: Gen. 228 (2002) 135.
[60] W.C. Conner Jr., J.L. Falconer, Chem. Rev. 95 (1995) 759.
[61] A.-G. Boudjahem, S. Monteverdi, M. Mercy, D. Ghanbaja, M.M. Bettahar, Catal. Lett. 84 (2002) 115.
[62] V.I. Bogillo, L.S. Pirnach, A. Dabrowski, Langmuir 13 (1997) 928.
[63] R.J. Iwanowski, M. Heinonen, I. Pracka, J. Kachniarz, Appl. Surf. Sci. 136 (1998) 95.
[64] B.A. Riguetto, S. Damyanova, G. Gouliev, C.M.P. Marques, L. Petrov, J.M.C. Bueno, J. Phys. Chem. B 108 (2004) 5349.
[65] A. Talo, J. Lahtinen, P. Hautojärvi, Appl. Catal. B: Environ. 5 (1995) 221.
[66] F. Mercier, C. Alliot, L. Bion, N. Thromat, P. Toulhoat, J. Electron Spectros. Relat. Phenom. 150 (2006) 21.
[67] Q.J. Cai, Q.D. Ling, S. Li, F.R. Zhu, W. Huang, E.T. Kang, K.G. Neoh, Appl. Surf. Sci. 222 (2004) 399.
[68] G. Tavoularis, M.A. Keane, J. Mol. Catal. A: Chem. 142 (1999) 187.
[69] F.J. Berry, L.E. Smart, P.S.S. Prasad, N. Lingaiah, P.K. Rao, Appl. Catal. A: Gen. 204 (2000) 191.
[70] A.R. Suzdorf, S.V. Morozov, N.N. Anshits, S.I. Tsiganova, A.G. Anshits, Catal. Lett. 29 (1994) 49.
[71] E.-J. Shin, M.A. Keane, Appl. Catal. B: Environ. 18 (1998) 241.
[72] C. Menini, G. Tavoularis, C. Park, M.A. Keane, Catal. Today 62 (2000) 355.
[73] B.F. Hagh, D.T. Allen, Chem. Eng. Sci. 45 (1990) 2695.
[74] J. Estellé, J. Ruz, Y. Cesteros, R. Fernández, P. Salagre, F. Medina, J.-E. Suegras, J. Chem. Soc., Faraday Trans. 92 (1996) 2811.
[75] W.C. Martin, A. Musgrove, S. Kotochigova, J.E. Sansonetti, Ground Levels and Ionization Energies for the Neutral Atoms, Version 1.3, National Institute of Standards and Technology, Gaithersburg, MD, 2003.
[76] S.P. Ionov, N.T. Kuznetsov, Russ. J. Coord. Chem. 26 (2000) 887.
[77] R. Gopinath, N. Lingaiah, B. Sreedhar, I. Suryanarayana, P.S.S. Prasad, A. Obuchi, Appl. Catal. B: Environ. 46 (2003) 587.
[78] S. Ordóñez, H. Sastre, F.V. Díez, Appl. Catal. B: Environ. 40 (2003) 119.
[79] C. Park, C. Menini, J.L. Valverde, M.A. Keane, J. Catal. 211 (2002) 451.
[80] G. Yuan, M.A. Keane, Chem. Eng. Sci. 58 (2003) 257.